"汪闻韶院士青年优秀论文奖"

申请表

论文题目	Quantitative damage evaluation of concrete suffered freezing–thawing by DIP technique		
发表的期刊	Construction and Building Materials	发表时间	2014 年 8 月
论文作者	Shuguang Li, Gaixin Chen*, Guojin Ji, Yihui Lu		
第一作者	Shuguang Li（李曙光）	出生年月	1981.6
工作单位	中国水科院材料所	职务/职称	高工
联系电话	01068781415	手机号	13810103274
电子邮件	lisg@iwhr.com		
单位推荐意见	当前混凝土损伤评价方法均为无损评价法，无法反映混凝土损伤老化的本质，本文提出了基于数字图像处理技术和混凝土微裂纹量化分析技术的损伤评价方法。对冻融过程中引气和非引气混凝土的微裂纹萌生扩展过程进行了定量分析，揭示了混凝土冻融损伤微裂纹的演化规律，并初步建立了混凝土宏观性能演化与微裂纹演化之间的对应关系，初步提出了基于微裂纹密度的混凝土损伤程度评价方法。本文提供的方法为科学合理地评价混凝土的老化损伤、研究混凝土的劣化破坏机理提供了一个有利工具，具有重要的科学意义。审稿人评语为 "Good paper! Comprehensive and thoughtful work! Useful results!"。自 2014 年 8 月在线发表以来，已被国内外同行下载 230 次，其中 56% 为国外下载，充分显示了该论文的科学意义和国际影响力。 　　同意本文推荐申请汪闻韶院士青年优秀论文奖！ 　　　　　　　　　　　　　　　　　单位盖章 　　　　　　　　　　　　　　年　　月　　日		

Article Usage Dashboard
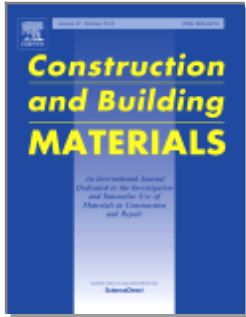
Quantitative damage evaluation of concrete suffered freezing-thawing by DIP technique

Li, S.; Chen, G.; Ji, G.; Lu, Y.

View Article

Views by geography

Top countries	Rank	Views	Pct
China	1	100	44%
United States	2	39	17%
United Kingdom	3	15	7%
Thailand	4	7	3%
Japan	5	7	3%

Trend and cumulative views

228 total views

Aug-14	Sep-14	Oct-14	Nov-14	Dec-14	Jan-15	Feb-15
36	33	43	43	17	26	30

Corporate versus Public Sector
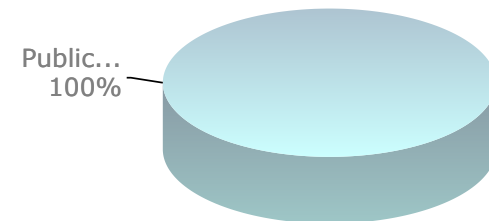
Public... 100%

Terms and conditions   Support

Construction and Building Materials
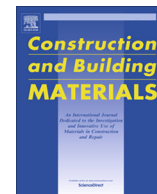
Quantitative damage evaluation of concrete suffered freezing–thawing by DIP technique

Shuguang Li, Gaixin Chen *, Guojin Ji, Yihui Lu

State Key Laboratory of Simulation and Regulation of Water Cycle in River Basin, China Institute of Water Resources and Hydropower Research, Beijing, China

HIGHLIGHTS

- FT-caused microcracking in concrete w/& w/o air-entrainment is studied by DIP.
- Matrix microcrack characteristics all increase with the increase of FT damage degree.
- ITZ cracks instead of mortar cracks are the major part of FT-caused cracks.
- FT-caused microcracks in concrete w/& w/o air-entrainment are compared.
- Relationships between mechanical properties and microcrack densities are established.

ARTICLE INFO

ABSTRACT

Most of the hydraulic concrete structures in cold regions of China are suffering freezing–thawing (FT) deterioration and the first step to choose repairing measures is to appropriately and quantitatively evaluate the FT damage degree in concrete. The current evaluating parameters for FT damage in concrete, such as resonant frequency and ultrasonic wave velocity are all phenomenological descriptions and cannot reveal the essence of the FT damage, which is the initiation and propagation of microcracks. This paper proposes a method to evaluate FT-damage in concrete based on vacuum–epoxy-impregnation method and digital-image-processing (DIP) technique. Quantitative microcrack analysis and mechanical tests including compressive tests, flexural tests and axial tensile tests were performed for the concrete specimens with/without air-entrainment suffered different FT cycles. Evolutions of microcrack characteristics of the matrix cracks (including Interfacial Transition Zone (ITZ) cracks and mortar cracks) in the concrete specimens were thoroughly investigated. Relationships between the relative mechanical properties and the microcrack density were established. Results show that the length density, area density and crack width of microcracks in the matrix of concrete all increase with the increase of damage degree and the ITZ cracks instead of the mortar cracks are the major part of FT-caused microcracks. The high correlation coefficients between the mechanical properties and microcrack density indicate that quantitative microcrack analysis could be used as a powerful and promising tool of quantifying FT damage in concrete.

1. Introduction

Most of the hydraulic concrete structures in North China are subjected to freezing and thawing (FT) deteriorations because of the cold weather and severe/rapid temperature changes all year around. FT-damaged concrete will suffer mass loss, decreases in mechanical properties and gradual loss of durability caused by microcrack development [1,2]. The precondition of maintaining and repairing FT-damaged concrete structures is to make appropriate and reliable evaluations for the damage in concrete. The most effective and essential way to evaluate FT damage in concrete is to quantify the microcracking process in the FT process and establish the property–microstructure relationships. However, the current three widely-used FT-damage evaluating parameters, namely the resonant frequency [3,4], the ultrasonic wave velocity [3,5,6] are all phenomenological damage descriptions and neither can directly reveal the initiation and growth process of microcracks in concrete. Though CT technology seems to be a promising non-destructive tool to get the 3D structure of cracks in concrete through image-reconstruction, the spatial resolution and field of interest are in a dilemma and it is really

* Corresponding author. Address: A1 Fuxing Road, Haidian District, Beijing 100038, China. Tel.: +86 10 68781469; fax: +86 10 68529680.
E-mail address: chengx@iwhr.com (G. Chen).

Table 1
Chemical composition of cement.

Chemical composition	SiO$_2$	Al$_2$O$_3$	Fe$_2$O$_3$	CaO	MgO	K$_2$O	Na$_2$O	SO$_3$	Loss on ignition
Cement (%)	21.42	3.51	5.32	60.55	4.76	0.39	0.10	2.28	0.64

Table 2
Mixing proportion of non-air-entrained concrete (NAC) and air-entrained concrete (AC).

	W/C	Sand ratio (%)	Super-plasticizer (%)	Air-entraining agent (%)	Water (kg/m^3)	Cement (kg/m^3)	Fly ash (kg/m^3)	Sand (kg/m^3)	Aggregate (kg/m^3)	
									5–20 mm	20–40 mm
NAC	0.45	36	0.60	/	140	311	/	719	510	765
AC	0.45	36	0.60	0.01	122	230.4	40.7	745	528	793
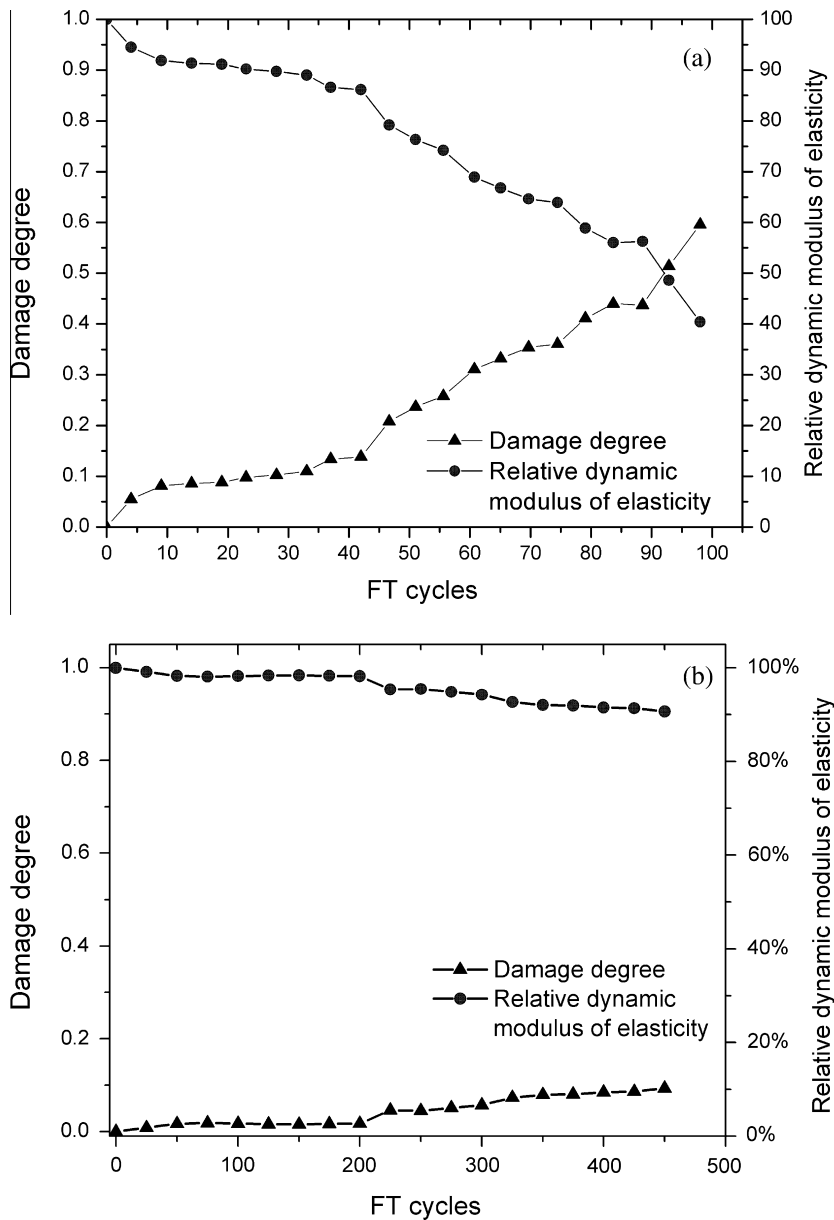
Fig. 1. Relative dynamic modulus of elasticity and FT damage degree of non-air-entrained concrete (a) and air-entrained (the air content is 5%) concrete (b) at different FT cycles.

a huge challenge for the current CT system to detect FT-caused microcracks 10–50 μm wide in full-scale concrete specimens which are usually over 5 cm in dimension in the laboratory. For instance,

Wakimoto [7] applied X-ray laminography to assess frost-damage in concrete specimens 7.6 cm in dimensions, but only microcracks about 0.1–0.2 mm in width could be identified. Though Promentilla

Table 3
Mechanical properties of non-air-entrained concrete specimens suffered different FT cycles.

Concrete specimens	S_0	S_1	S_2	S_3	S_4	S_5	S_6
FT cycles	0	27	44	74	85	91	98
FT damage degree, D_{FT}	0	0.083	0.161	0.329	0.398	0.441	0.596
Compressive strength/MPa	62.6	60.6	59.1	56.3	52.3	48.5	45.7
Relative compressive strength	1.000	0.969	0.943	0.899	0.836	0.775	0.730
Flexural strength/MPa	5.87	4.78	4.31	3.19	2.50	2.04	1.62
Relative flexural strength	1	0.810	0.727	0.533	0.415	0.339	0.271
Axial tensile strength/MPa	3.06	2.81	2.62	1.66	1.26	1.13	1.05
Relative axial tensile strength	1	0.897	0.816	0.493	0.369	0.324	0.299

Table 4
Mechanical properties of air-entrained concrete specimens suffered different FT cycles.

Concrete specimens	A0	A1	A2	A3	A4	A5
FT cycles	0	200	300	350	400	450
FT damage degree, D_{FT}	0	0.018	0.057	0.080	0.084	0.092
Compressive strength/MPa	42.6	42.1	41.4	39.0	38.9	38.8
Relative compressive strength	1.000	0.988	0.972	0.915	0.913	0.911
Flexural strength/MPa	5.63	4.72	4.02	4.04	3.98	3.93
Relative flexural strength	1.000	0.838	0.714	0.718	0.708	0.698
Axial tensile strength/MPa	2.82	2.47	2.11	2.09	2.09	2.09
Relative axial tensile strength	1.000	0.876	0.748	0.741	0.741	0.741

and Sugiyama [8] detected microcracks as small as 10 μm in width in mortar specimens exposed to FT by microfocus X-ray CT system, the cylindrical specimen he scanned was only 12 mm in diameter.

With the development of microscopy and digital-image-processing (DIP) techniques, quantifying microcracks in deteriorated cementitious materials becomes feasible now [9–13]. This paper firstly presented a method of identification and quantification of microcracks in concrete based on vacuum-epoxy-impregnation method and DIP technique. Secondly evolutions of microcrack patterns of mortar cracks, ITZ cracks and matrix cracks (composed of ITZ cracks and mortar cracks) in non-air-entrained and air-entrained concrete with the increase of FT cycles were investigated. Finally relationships between the mechanical properties and the microcrack density were established.

2. Experimental program

2.1. Materials and mixing proportion

Two groups of concrete specimens (non-air-entrained and air-entrained) were produced and medium-heat Portland cement P. MH42.5 in China (equivalent to ASTM Type II) with a density of 3.23 g/cm³ and type I fly ash with a density of 2.39 g/cm³ were used was used and the chemical compositions were shown in Table 1.

Crushed sand was used as fine aggregates with a density of 2.60–2.63 g/cm³, a fineness modulus of 2.77–2.97 and a water absorption ratio in saturated-surface-dry (S.S.D) condition of 1.0–1.4%.

Crushed gravels whose sizes were in the ranges of 5–20 mm and 20–40 mm respectively were used as coarse aggregates. A naphthalene-based superplasticizer was applied to produce fresh concrete with satisfying workability. Rosin-based air-entraining agent was used for air-entrained concrete and the actual air void content in the concrete specimens is 5.0 ± 0.5%.

The mixing proportions of the two series of concrete are shown in Table 2.

2.2. Testing procedure

A series of prismatic, cubic and cylindrical specimens were produced for either non-air-entrained or air-entrained concrete for FT tests and mechanical tests according to the *Test code for hydraulic concrete (SL352-2006)* of China. After being cured for 28 d in the standard curing room, all the specimens were sealed in silver-paper bags filled with water and kept in the chamber of the FT testing machine. Rapid freezing and thawing methods were used and the resonant frequency tests of the specimens at different FT cycles were done according to the *Test code for hydraulic concrete (SL352-2006)*, which is similar with the *Standard Test Method for Resistance of Concrete to Rapid Freezing and Thawing (ASTM C 666 M-03)*.

Mechanical tests were performed to get the compressive strength, the flexural strength and the axial tensile strength of those specimens subjected to different FT cycles. The dimensions of the specimens for the compressive tests and axial tensile
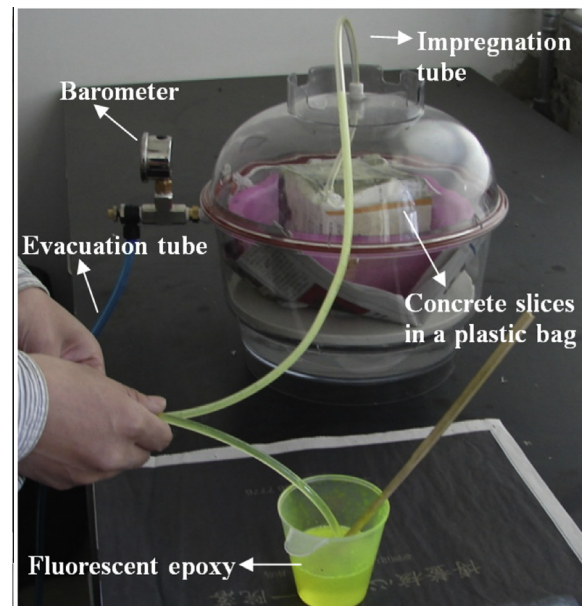
(a)
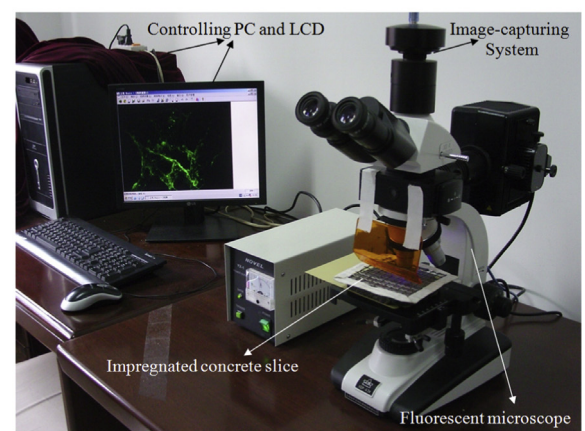
(b)

Fig. 2. The vacuum impregnation system (a) and the fluorescent microscope system (b).
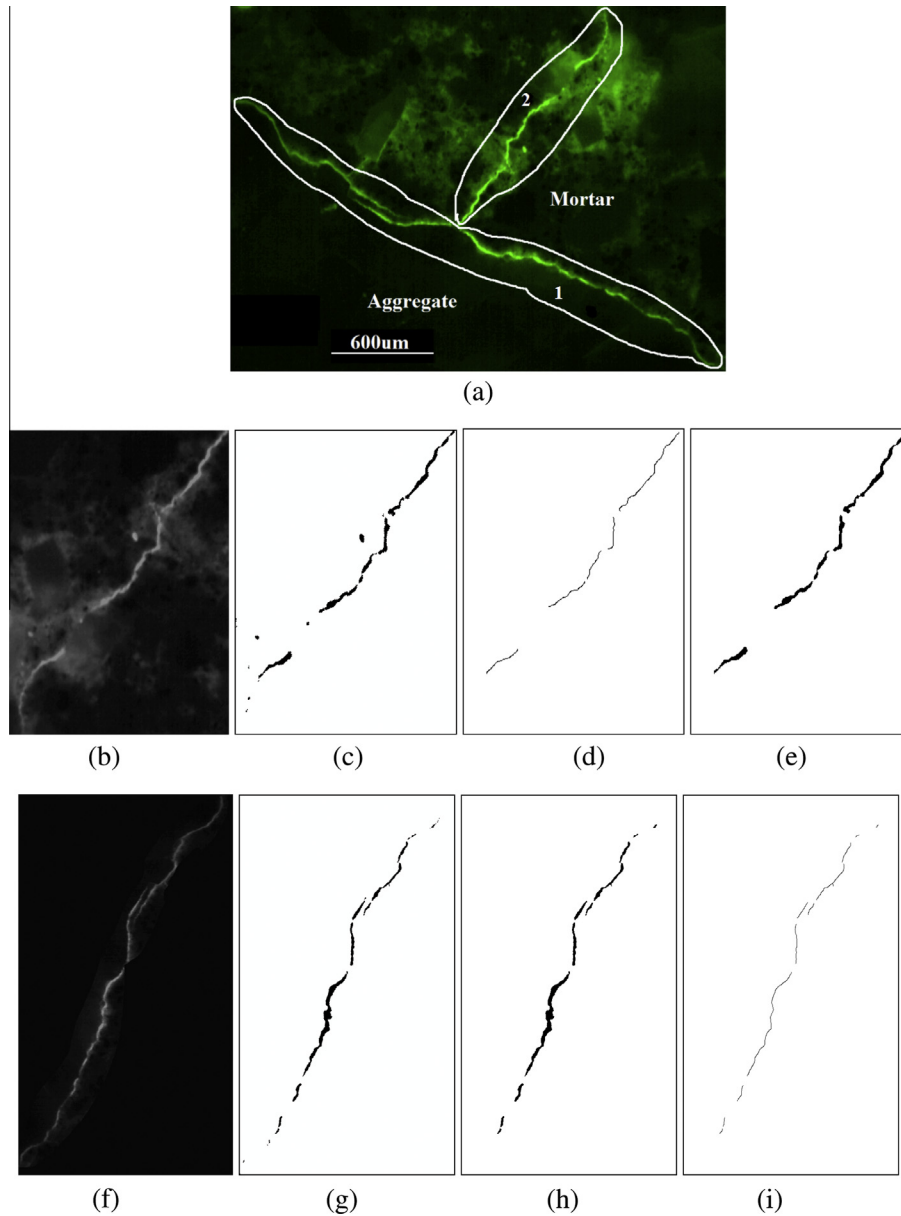
Fig. 3. Typical microcrack image including ITZ crack (circle 1 in (a)) and mortar crack (circle 2 in (a)); processing flowchart of typical mortar crack image (b–e) and ITZ crack image (f–i) by QUANSMIC: grayscale images (b, f); binary images after thresholding (c, g); images after shape analysis (d, h); skeletons of the microcracks (e, i).

tests were 15 cm × 15 cm × 15 cm and 10 cm × 10 cm × 55 cm, respectively. For the resonant frequency tests as well as the flexural tests the specimen dimensions were 10 cm × 10 cm × 40 cm.

2.3. Freezing–thawing and mechanical test results

FT damage degree is proposed to describe the deteriorating extent of FT cycles to concrete and it is calculated by the following formula,

$$D_{FT} = 1 - \frac{E'}{E_0}, \tag{1}$$

where D_{FT} is the FT damage degree, E_0 is the initial dynamic modulus of elasticity of concrete and E' is the dynamic modulus of elasticity of concrete suffered certain FT cycles.

The relative dynamic modulus of elasticity and FT damage degree of the non-air-entrained and air-entrained concrete specimens at different FT cycles are shown in Fig. 1(a) and (b). It can be seen from Fig. 1(a) and (b) that for both groups of concrete the relative dynamic modulus of elasticity decreases while the FT damage degree increases with the increase of FT cycles.

For non-air-entrained concrete the FT damage degree firstly increases slowly before 45 FT cycles and then rapidly increases to around 0.60 at 98 FT cycles (see Fig. 1(a)), while for air-entrained concrete the FT damage degree increases approximately linearly to only around 0.10 at 450 FT cycles (see Fig. 1(b)). The comparison shows that the frost resistance of air-entrained concrete with an air content of 5.0% is satisfactorily higher than non-air-entrained concrete.

Tables 3 and 4 show the FT damage degree, the relative compressive strength, the relative flexural strength and the relative axial tensile strength of non-air-entrained and air-entrained concrete specimens suffered different FT cycles, respectively. The relative mechanical properties are calculated by dividing the mechanical properties of concrete specimens suffered certain FT cycles by those cured in the standard curing room for 28 d.

It can be seen from Tables 3 and 4 that the relative compressive strength, the relative flexural strength and the relative axial tensile strength of the concrete specimens without and with air-entrainment all decrease with the increase of FT cycles. Also it can be seen that the flexural strength and the axial tensile strength of concrete are more sensitive to FT damage than the compressive strength. Take the non-air-entrained concrete specimens for example, it can be seen from Table 3 that the relative compressive strength only decreases to 0.730 while the relative flexural strength and the relative axial tensile strength decrease to 0.271 and 0.299 respectively at the FT cycle number of 98.
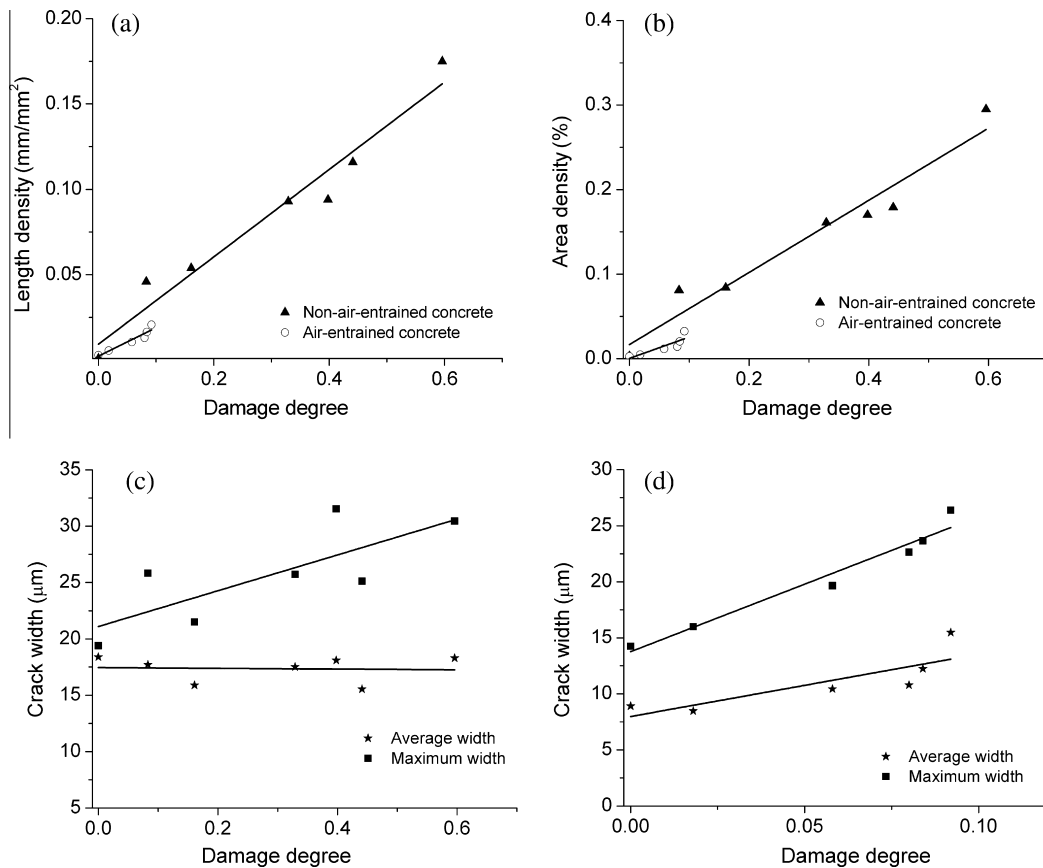
Fig. 4. Evolutions of the length density (a) and area density of matrix cracks with FT damage degree in non-air-entrained concrete and air-entrained concrete; evolutions of the average width and maximum width of matrix cracks with FT damage degree in non-air-entrained concrete (c) and air-entrained concrete (d).

3. Quantitative microcrack analysis

Quantitative microcrack analyses were performed on those slices cut from the specimens tested for resonant frequencies at specified FT cycles.

3.1. Specimen preparation

The concrete specimens for microscopic analysis were prepared by fluorescent-epoxy vacuum-impregnation method in the following procedures:

a. Two slices of 15–20 mm thickness were cut from the middle parts of each 10 cm × 10 cm × 40 cm prismatic specimen (to reduce the effects of both ends on microcrack patterns) which had been tested for resonant frequency at different FT cycles.
b. The surfaces of the slices were ground and polished using a grinder to obtain a smooth flat surface.
c. The smooth surfaces were rinsed with water at low and high speeds to remove any leftover debris.
d. The slices were dried in an oven at a temperature of 40–50 °C for 24 h (According to Gran's experimental results [14], the effect of being dried at 50 °C on the cracking extent in the concrete slices is not significant).
e. The slices were placed in a plastic container and evacuated for at least 1 h at a constant pressure of 1 kPa in a vacuum chamber.
f. The plastic container inside the vacuum chamber was then filled with the epoxy resin containing fluorescent dye while maintaining the vacuum (see Fig. 2(a)).

g. Finally, the slices were taken out from the vacuum chamber and from the plastic container, and then slightly ground to remove the excess epoxy on the surfaces once the epoxy was hardened.

3.2. Quantitative analysis system of microcracks in concrete

Besides specimen preparation, reliable quantitative analysis of microcracks requires acquisition, processing, and analysis of a large number of microscopic images because of the complexity and heterogeneity of the mesoscale structures of concrete. The impregnated and polished concrete slices, namely the microscopic specimens, were observed under a fluorescent microscopy to search for microcracks and have the images stored in the computer for further processing and analyzing (see Fig. 2(b)). The microscopic specimens were covered by a steel mesh which had a grid size of 1 cm × 1 cm and was helpful to seek and locate the microcracks. The specimens were scanned manually grid by grid on the stage at a magnification of 40 which was sufficient to detect microcracks as thin as 2 μm in width. Every grid was carefully observed to find all the microcracks inside and the total observed area for each slice took up as high as 90% of the slice's total area.

A MATLAB-based software package called QUANSMIC (Quantitative Analysis System of Microcracks in Concrete) was developed to acquire the geometrical characteristics of microcrack patterns. It includes four modules, namely image-binarizing module, shape-analyzing module, crack-skeletonizing module and automatic-measuring module. The original colour microscopic images containing microcracks are firstly converted into greyscale images, and then the microcracks are recognized and extracted by the image-binarizing module. Noises and voids are distinguished from
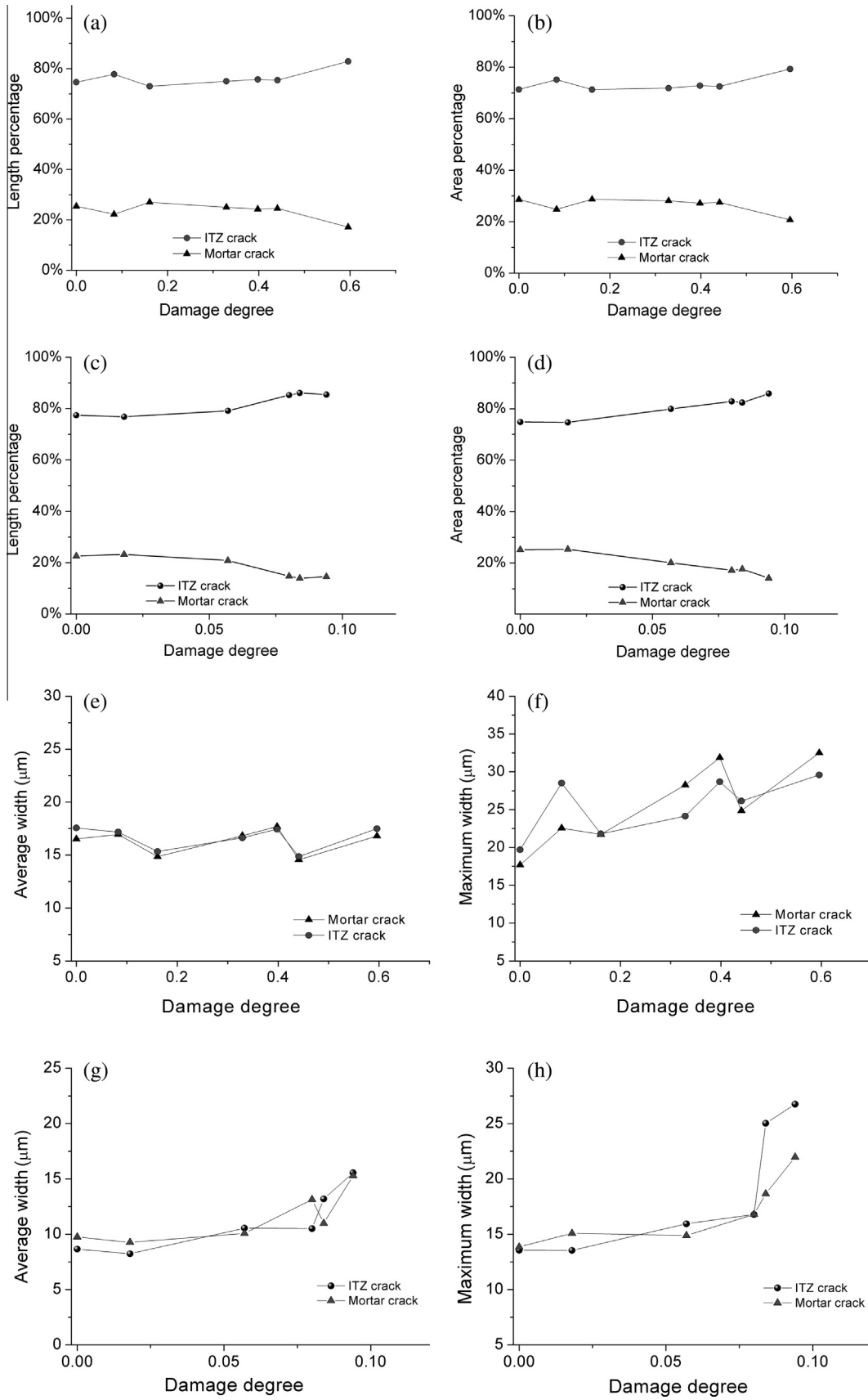
Fig. 5. Evolutions of the length percentage (a), area percentage (b), average width (e), and maximum width (f) of ITZ cracks and mortar cracks with FT damage degrees in non-air-entrained concrete; Evolutions of the length percentage (c), area percentage (d), average width (g), and maximum width (h) of ITZ cracks and mortar cracks with FT damage degrees in air-entrained concrete.
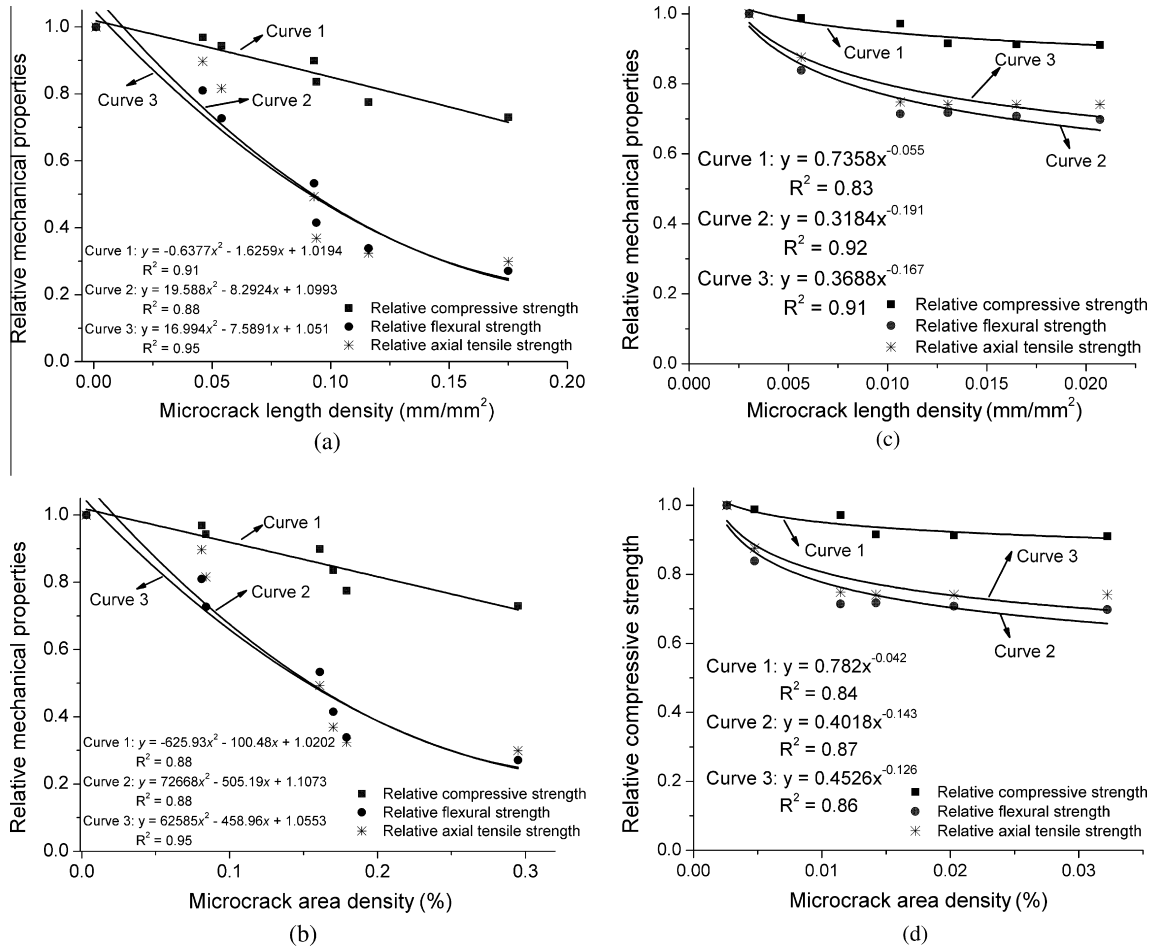
Fig. 6. Relationships between the relative mechanical properties and the length density (a) and the area density (b) of matrix cracks in non-air-entrained concrete; Relationships between the relative mechanical properties and the length density (c) and the area density (d) of matrix cracks in air-entrained concrete. Curve 1, 2 and 3 are fitted curves for the relative compressive strength, relative flexural strength and relative axial tensile strength respectively.

the microcracks and deleted by the shape-analyzing module and then the preserved microcracks are skeletonized by the crack-skeletonizing module. Finally the geometrical characteristics such as area, length and average width of the microcracks are measured and calculated by the automatic-measuring module. The processing flowchart of a typical microcrack image by QUANSMIC is shown in Fig. 3(a)–(i).

The precision of QUANSMIC was validated with several ordered specimens with shapes of known sizes (the precision of the ordered specimens is ±1 μm) and the relative errors of QUANSMIC were smaller than 5%, indicating it has a high accuracy [12].

4. Results and discussion

Six microcrack characteristic parameters, namely the total length/length density, the total area/area density, the maximum width and average width are calculated by QUANSMIC to quantify the microcrack patterns in concrete specimens subjected to different FT degrees. They are calculated as follows:

Total length – sum of the microcrack lengths on all the microscopic images.
Length density – ratio of the total length to the observing area.
Total area – sum of the microcrack areas on all the microscopic images.
Area density – percentage of the total area of microcracks to the observing area.

Average width – total area divided by the total length.
Maximum width – the maximum value of all the average microcrack widths.

4.1. Evolutions of the microcrack characteristics of the matrix cracks with different damage degrees

In this paper it is hypothesized that coarse aggregates are not affected by FT, so only matrix cracks (composed of ITZ cracks and mortar cracks) are analyzed.

The evolutions of the matrix microcrack density (the length density and the area density), matrix microcrack width (the average width and maximum width of matrix cracks) in the non-air-entrained and air-entrained concrete with FT damage degrees are shown in Fig. 4(a)–(d).

It can be seen from Fig. 4(a) and (b) that either the length density or the area density increases with the increase of the FT damage degree for both groups of concrete. As the damage degree increases from 0.0 to around 0.6, the length density and area density increase from around 0 to 0.175 mm/mm^2 and 0.295% respectively for non-air-entrained concrete. For air-entrained concrete, as the damage degree increases from 0 to close to 0.1, the length density and area density increase from around 0 to 0.0207 mm/mm^2 and 0.032% respectively.

Although the matrix microcrack density in air-entrained concrete seems a little smaller than non-air-entrained concrete at the same damage degree which is no more than 0.10 (as seen from
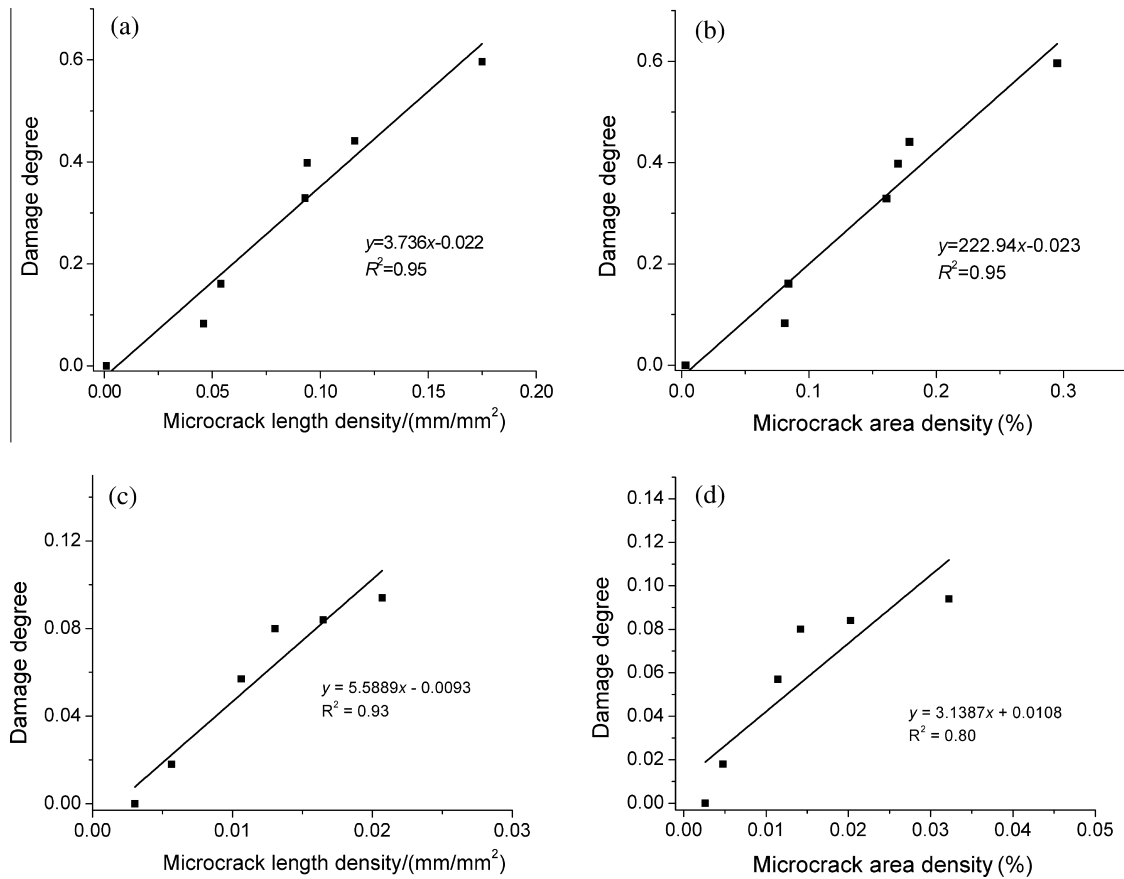
Fig. 7. Relationships between the FT damage degree and the length density (a) and the area density (b) of matrix cracks in non-air-entrained concrete; relationships between the FT damage degree and the length density (c) and the area density (d) of matrix cracks in air-entrained concrete.

Fig. 4(a) and (b)), more tests are needed to verify whether this applies to damage level greater than 0.10.

It can be seen from Fig. 4(c) and (d) that both the maximum width and the average width of matrix cracks increase with the increase of FT damage degree and the increasing slope of maximum crack width is greater than average crack width for both groups of concrete (For non-air-entrained concrete the average crack width remained almost unchanged during FT deteriorating process). The reason is probably that while the existing microcracks become wider and wider as the FT damage increases, many new microcracks are emerging making the average width of all the microcracks changed a little.

4.2. Evolutions of the microcrack characteristics of mortar cracks and ITZ cracks with different damage degrees

Evolutions of the length percentage/area percentage of the mortar cracks as well as ITZ cracks to the total matrix cracks are shown in Fig. 5(a)–(d), respectively. As can be seen from Fig. 5(a)–(d), for non-air-entrained and air-entrained concrete either the length percentage or area percentage of ITZ cracks is greater than 70%, which is much higher than mortar cracks taking less than 30% of total matrix cracks. It indicates that ITZ cracks are the major part of FT-caused microcracks in both groups of concrete. The reason why ITZ cracks are dominant in FT-caused microcracks relates closely with the difference between the linear thermal expansion coefficients of aggregates, ITZ and mortar, as well as ITZ's higher porosity and lower tensile strength compared with mortar [15–17].

The evolutions of the average width and maximum width of ITZ cracks and mortar cracks in both groups of concrete are shown in Fig. 5(e)–(h) respectively. It can be seen from Fig. 5(e)–(h) that as

the FT damage degree increases, either the average width or the maximum width of both mortar cracks and ITZ cracks in concrete air-entrained or not has the trend of increasing. It can also be seen that there are no obvious differences between the ITZ cracks and mortar cracks in either average width or maximum width for non-air-entrained and air-entrained concrete.

4.3. Relationships between the macro properties and matrix microcrack density of FT damaged concrete

Relationships between the mechanical properties (including the relative compressive strength, the relative flexural strength and the relative axial tensile strength) and the matrix microcrack density (length density/area density of the matrix cracks) in non-air-entrained and air-entrained concrete are shown in Fig. 6(a)–(d), respectively.

It can be seen from Fig. 6(a), (b) and Fig. 6(c), (d) that good quadratic and power correlations can be established between the relative mechanical properties and the matrix microcrack density in non-air-entrained and air-entrained concrete, respectively. All the squares of the correlation coefficients are no less than 0.83. It can also be seen from Fig. 6(a)–(d) that the relative compressive strength is less sensitive to the microcrack density than the relative flexural strength and the relative axial tensile strength, which are both sensitive to the FT damage degree and the fitted curves almost overlap.

Relationships between the FT damage degree and the matrix microcrack density in non-air-entrained and air-entrained concrete are shown in Fig. 7(a), (b) and Fig. 7(c), (d) respectively.

It can be seen from Fig. 7(a)–(d) that good linear relationships can be established between the damage degree and the matrix

microcrack density, although the correlation coefficients for air-entrained concrete is not as high as non-air-entrained concrete. This is probably because of the narrow range of the data series for air-entrained concrete whose maximum FT damage degree is just around 0.10.

As seen from the above results and analyses, the decreases in the mechanical properties of FT-deteriorated concrete have strong correlations with the matrix microcrack density. This indicates that instead of mechanical tests and non-destructive tests to measure the resonance frequency or the ultrasonic velocity, microcrack density obtained by quantitative microcrack analysis could be developed as a new tool to quantitatively evaluate FT damage in concrete. Anyway, correlations between the macro properties and the microcrack density established in this section are just preliminary results showing a high probability of quantifying FT damage in concrete by microcrack characteristics.

5. Conclusions

A thorough investigation based on DIP techniques was made on the development of microcrack patterns in slices cut from non-air-entrained and air-entrained concrete specimens suffered different FT cycles. The following conclusions can be drawn from the results and analysis above.

a. The length density, area density, crack width of matrix cracks all increase with the increase of FT damage degree in concrete whether air entrained or not.

b. ITZ cracks instead of mortar cracks are the major part of FT-caused microcracks in concrete and there are no obvious differences in average width or maximum width between the matrix cracks and ITZ cracks.

c. Good correlations are established between the macro properties (including the relative compressive strength, the relative flexural strength, the relative axial tensile strength and the FT damage degree) and the matrix microcrack density (the length density and the area density), indicating that microcrack density could be used as a direct and visual parameter to evaluate FT damage in concrete.

d. The matrix microcrack density of air-entrained concrete seems smaller than that of non-air-entrained concrete at the same damage degree which is no more than 0.10. It needs to be verified by more tests whether this applies to damage level greater than 0.10.

Results of this study indicate that quantitative microcrack analysis is a powerful and promising tool to quantify FT damage in concrete. More work needs to be done to study the spatial distributions of microcracks in the FT-affected prismatic concrete specimens and to study the long-term evolution of microcrack characteristics with FT damage degree. The effects of air void content, aggregate type on the development of microcrack characteristics also need to be studied in the future.

Appendix A

Notation:

D_{FT}	damage degree in concrete caused by freezing–thawing
E'	elastic modulus of damaged concrete
E_0	elastic modulus of undamaged concrete

References

[1] Jacobsen S, Marchand J, Hornain H. SEM observations of the microstructure of frost deteriorated and self-healed concretes. Cem Concr Res 1995;25:1781–90.

[2] Wardeh G, Mohamed MA, Ghorbel E. Analysis of concrete internal deterioration due to frost action. J Build Phys 2011;35:54–82.

[3] Ohtsu M. Damage evaluation in freezing and thawing test of concrete by elastic-wave methods. Mater Struct 2011;44:1725–34.

[4] China Institute of Water Resources and Hydropower Research. Test code for hydraulic concrete, SL 352-2006; 2006 [in Chinese].

[5] Suzuki T, Ogata H, Takada R, Aoki M, Ohtsu M. Use of acoustic emission and X-ray computed tomography for damage evaluation of freezing and thawed concrete. Constr Build Mater 2010;24:2347–52.

[6] Molero M, Aparicio S, Al-Assadi G, Casati MJ, Hernández MG, Anaya JJ. Evaluation of freeze–thaw damage in concrete by ultrasonic imaging. NDT and E Int 2012;52:86–94.

[7] Wakimoto K, Blunt J, Carlos C, Monteiro PJM, Ostertag CP, Albert R. Digital laminography assessment of the damage in concrete exposed to freezing temperatures. Cem Concr Res 2008;10:1232–45.

[8] Promentilla MAB, Sugiyama T. X-ray microtomography of mortars exposed to freezing-thawing action. J Adv Concr Technol 2010;8:97–111.

[9] Ammouche A, Breysse D, Hornain H, Didry O, Marchand J. A new image analysis technique for the quantitative assessment of microcracks in cement-based materials. Cem Concr Res 2000;1:25–35.

[10] Litorowicz A. Identification and quantification of cracks in concrete by optical fluorescent microscopy. Cem Concr Res 2006;8:1508–15.

[11] Elzafraney M, Soroushian P. Sampling approach for quantitative microscopic investigation of concrete through planar and spatial measurements. Mag Concr Res 2005;6:321–30.

[12] Li S, Chen G, Lu Y. Quantitative damage evaluation of AAR-affected concrete by DIP technique. Mag Concr Res 2013;65(5):332–42.

[13] Soroushian P, Elzafraney M, Nossoni A. Specimen preparation and image processing and analysis techniques for automated quantification of concrete microcracks and voids. Cem Concr Res 2003;33(12):1949–62.

[14] Gran HC. Fluorescent liquid replacement technique–a means of crack detection and water:binder ratio determination in high strength concretes. Cem Concr Res 1995;25:1063–74.

[15] Simeonov P, Ahmad S. Effect of transition zone on the elastic behavior of cement-based composites. Cem Concr Res 1995;1:165–76.

[16] Akcaoglu T, Tokyay M, Celik T. Assessing the ITZ microcracking via scanning electron microscope and its effect on the failure behavior of concrete. Cem Concr Res 2005;2:358–63.

[17] Zheng JJ, Li CQ, Zhou XZ. Characterization of microstructure of interfacial transition zone in concrete. ACI Mater J 2005;4:265–71.